Electronic Supplementary Information

Morphology-controlled green synthesis of Tellurium Nanostructures and application of Te/MXene hybrid structure

Mengchen Xu,[a‡] Jinshu Li,[b‡] Qingshan Yang,[b] Lu Jiang,[a] Jiaqi He,[c] Dawei He*[a], Yongsheng Wang*[a] and Yajie yang*[a]

[a.] Key Laboratory of Luminescence and Optical Information, Ministry of Education, Institute of Optoelectronic Technology, Beijing Jiaotong University, Beijing 100044.

[b.] SKKU Advanced Institute of Nanotechnology (SAINT), Sungkyunkwan University, Suwon 16419, South Korea.

[c.] College of Mathematics and Physics, Beijing University of Chemical Technology, Beijing 100029, China

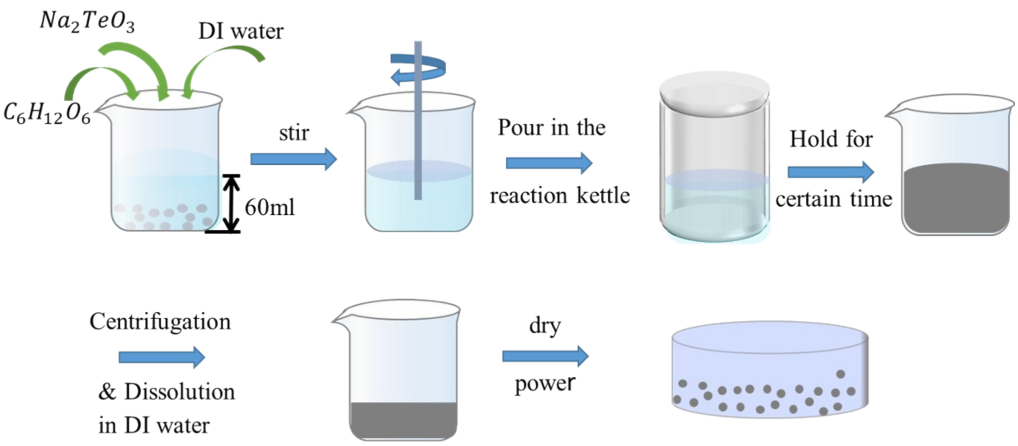

Figure S1. Experimental method and operation process of synthesizing Te NWs

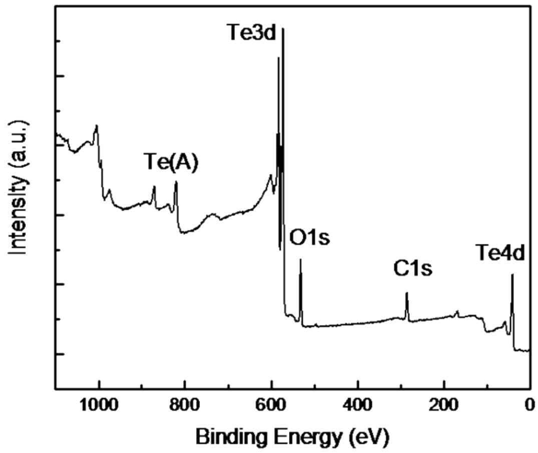

Figure S2. Wide-range XPS spectra of Te nanotube prepared at 90 ℃. Obvious Te 3d peaks are demonstrated by the XPS spectra of Te nanotubes, similar to those of Te nanowires.

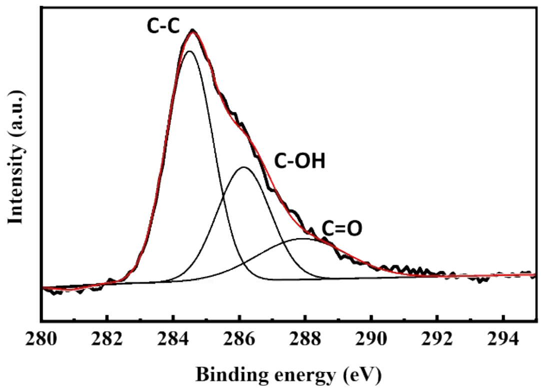

Figure S3. High-resolution XPS spectrum of the C 1s peak for Te/C nanocables.

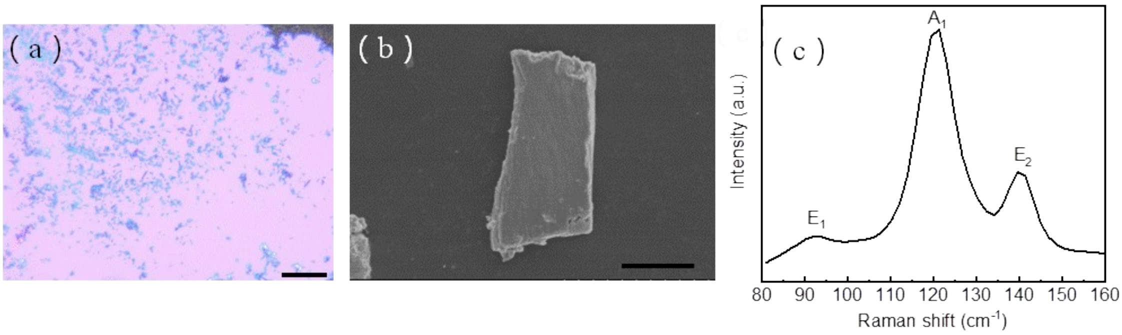

Figure S4. (a) OM image of the synthesized tellurene on SiO_2 substrate. Scale bar, 30 μm. (b) SEM image of synthesized tellurene. Scale bar, 5 μm. (c) Raman spectra of the synthesized tellurene.

The images in Figure S4 exhibit the characterizations of the synthesized 2D tellurene. F igure S4a is the OM image of tellurene on a SiO_2 substrate, in which various uniform 2D nanosheets were observed. The SEM image in Figure S4b confirms the lateral dimension of tellurene ～10 μm. Raman spectroscopy was used to explore the crystal structure of the o btained tellurene, and the spectra are shown in Figure S4c. Three active modes located at 92, 121, and 141 cm^{-1} are donated as the E1, A1, and E2 vibration modes, respectively, c onsistent with the reported works.[1-3]

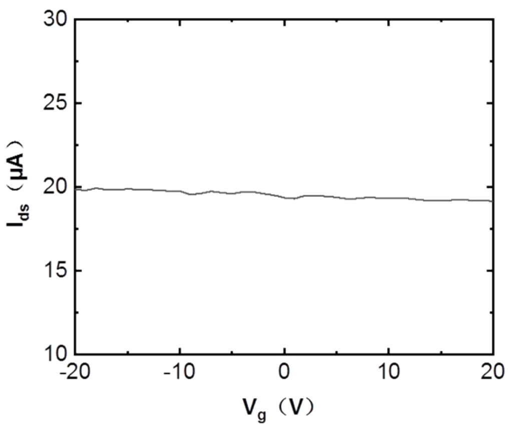

Figure S5. Transfer curve of the synthesized Te NWs film. V_d=0.1 V.

For the transfer curve in Figure S5, the drain current slightly changed with the increase of gate voltage from -20 V to 20 V, and high drain current could be obtained at low drain voltage, indicating the high metallic conductivity of Te NWs. As reported, high junction resistance exists between individuals in nanotube films[4] and the poorly conductive amorphous carbon shells of nanocables decrease the conductivity of Te nanocable film[5], so Te NWs were employed for the application of transparent conductive electrodes in this work.

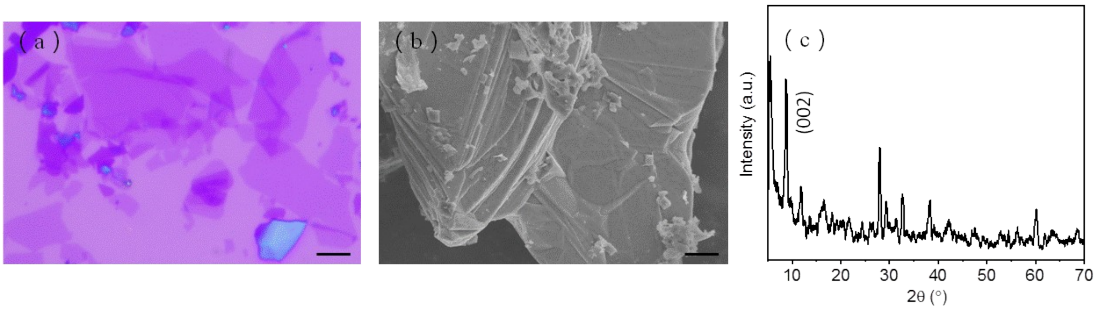

Figure S6. (a) OM image of the synthesized $Ti_3C_2T_x$ flakes on SiO_2 substrate. Scale bar, 2 um. (b) SEM images of synthesized tellurene. Scale bar, 2 μm. (c) XRD pattern of the synthesized $Ti_3C_2T_x$.

The investigations of the synthesized $Ti_3C_2T_x$ flakes are shown in Figure S6. The OM image in Figure S6a and SEM image in Figure S6b indicate the exfoliated large-area and thin $Ti_3C_2T_x$ flakes. The XRD pattern in Figure S6c further confirms the high quality of the achieved $Ti_3C_2T_x$ flakes, in which a weak peak at 39° is observed.[6, 7]

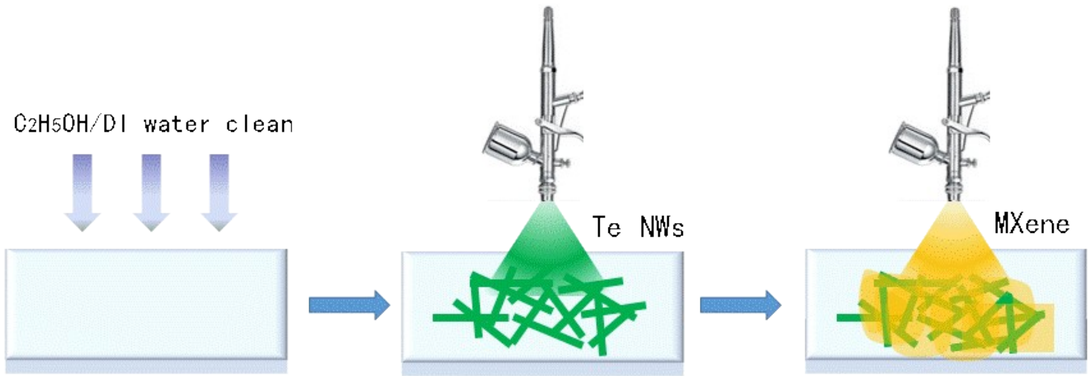

Figure S7. Schematic of the fabrication process of Te NWs/MXene hybrid structures.

Figure S7 is the schematic of fabricating Te NWs/MXene hybrid structure. Firstly, the substrate was cleaned with ethanol (C_2H_5OH) and deionized (DI) water. Then, in sequence, Te NWs and MXene solutions were spray-coated on the prepared substrate.

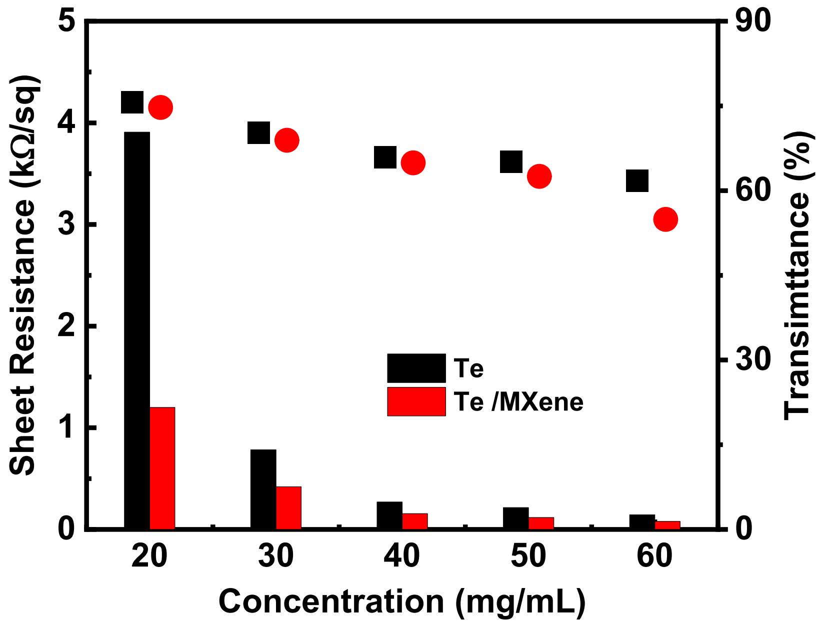

Figure S8. Sheet resistances and transmittances of Te and Te NWs/MXene hybrid structures with different solution concentrations of Te NWs.

The sheet resistances and transmittances at 550 nm of pure Te and Te NWs/MXene hybrid structures were measured and summarized in Fig. S8. With the spray-coating of the MXene layer, significant performance enhancements were demonstrated by Te/MXene hybrid structures with lower sheet resistances and similar transmittances. When the solution concentration of Te NWs is 10 mg/mL, the sheet resistance of Te film is difficult to measure, so 20 mg/mL is the minimum concentration investigated in this work.

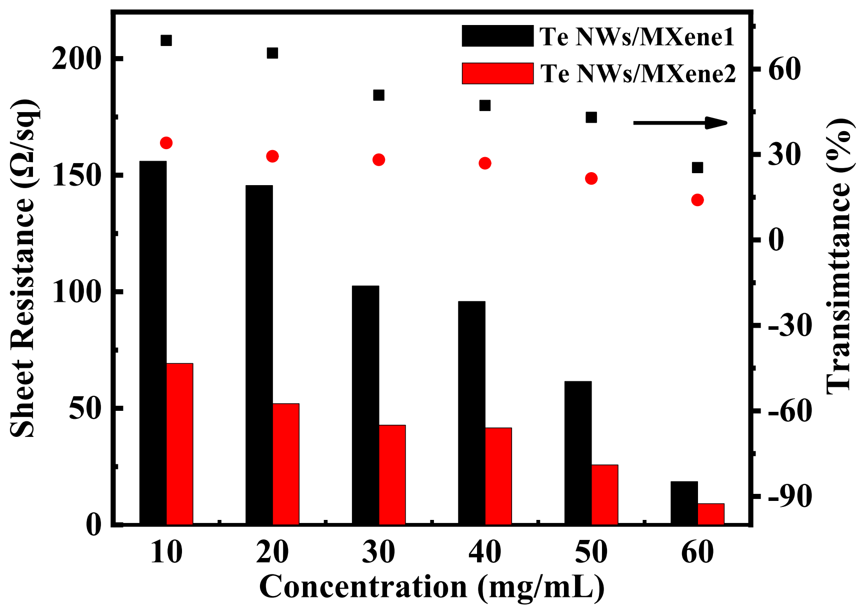

Figure S9. Sheet resistances and transmittances of Te NWs/MXene hybrid structure with different solution concentrations of MXene. Te NWs/MXene1: Te NWs/MXene hybrid structure with one layer of MXene. Te NWs/MXene2: Te NWs/MXene hybrid structure with two layers of MXene.

Table S1 A comparison of various transparent conductive electrodes.

Material	Method	Sheet resistance (Ω/sq)	Transmittance (%)	Refs.
$Ti_3C_2T_x$ in water	Spray-coating	1300	68	[8]
$Ti_3C_2T_x$ in ethanol	Spray-coating	3500	58	[8]
rGO	Filtration	565	59	[9]
graphene	CVD growth	280	80	[10]
Te/MXene	Spray-coating	156	70	This work

rGO: reduced graphene oxide.

Various transparent conductive electrodes based on nanomaterials are summarized in Table 1. Compared with pure $Ti_3C_2T_x$ TCEs, the Te/MXene hybrid structure shows a lower sheet resistance with a higher transmittance, which is supposed to be attributed to (1) the Te NWs distributed across the MXene flakes act as conductive bridges and reduce the contact resistance.[11] (2) the Te/MXene hybrid structure could be a resistivity in parallel problems, the total resistance of Te/MXene TCE is lower than every individual component in the hybrid conductive structures.[12] Therefore, compared to pure MXene film, Te/MXene hybrid TCE demonstrates a better performance.

References

1. Y. H. Jianting Lu, Churong Ma, Qiaojue Ye, Huaxin Yi, Zhaoqiang Zheng, and a. G. Y. Jiandong Yao, *Adv. Mater.*, 2023, **35**, 2211562.
2. G. Q. Yixiu Wang, Ruoxing Wang, Shouyuan Huang, Qingxiao Wang, Yuanyue Liu,, W. A. G. I. Yuchen Du, Moon J. Kim, Xianfan Xu, Peide D. Ye and and W. Wu, *Nature Electronics*, 2018, **1**, 228-236.
3. G. Liu, J. Yuan, T. Wu, F. Zhang, F. Xing, W. Zhang, H. Zhang and S. Fu, *IEEE J. Sel. Top. Quantum Electron.*, 2021, **27**, 1-6.
4. P. J. K. Sukanta De, Philip E. Lyons, Umar Khan, and Jonathan N. Coleman, *ACS nano*, 2010, **4**, 7064–7072.
5. W. X. a. S.-H. Yu, *Small*, 2009, **5**, 460–465.
6. H. Y. Shunlong Zhang, Pengfei Huang, Jianli Wang, Zhao Zhang, Tiantian Yang, and Wei-Qiang Han, *ACS nano*, 2020, **14**, 17665-17674.
7. H. L. Wanlin Feng, Yu Wang, Sifan Zeng, Lianwen Deng, Xiaosong Zhou, Haibin Zhang and Shuming Peng, *RSC Adv.*, 2018, **8**, 2398.
8. M.-Q. Z. Kanit Hantanasirisakul , Patrick Urbankowski , Joseph Halim , Babak Anasori , Sankalp Kota , Chang E. Ren , Michel W. Barsoum , and Yury Gogotsi *Adv. Electron. Mater.*, 2016, **2**, 1600050.
9. C. P. Dimitrios Konios , George Kakavelakis , Maria Sygletou , Kyriaki Savva , Emmanuel Stratakis , * and Emmanuel Kymakis *Adv. Funct. Mater.*, 2015, **25**, 2213–2221.
10. K. S. Kim, Y. Zhao, H. Jang, S. Y. Lee, J. M. Kim, K. S. Kim, J.-H. Ahn, P. Kim, J.-Y. Choi and B. H. Hong, *Nature*, 2009, **457**, 706-710.
11. J. Y. Su Ding, Fei Chen, Li Fu, Yanfei Lv, Shichao Zhao, Guoqiang Ji, *J. Nanopart. Res.*, 2021, **23**, 111.
12. W.-C. H. Tien-Chai Lin, Fu-Chun Tsai *Microelectron. Eng.*, 2017, **167**, 85–89.